Hindawi
Geofluids
Volume 2022, Article ID 3501755, 7 pages
https://doi.org/10.1155/2022/3501755

Research Article

Hydrate-Bearing Sediment Imaging of Ghost Reflection in Vertical Cable Seismic Data Using Seismic Interferometry

Linfei Wang,[1,2] **Zhong Wang**,[1] **Huaishan Liu**,[1,2] **Jin Zhang**,[1,2] **Lei Xing**,[1,2] **and Yanxin Yin**[1,2]

[1]*Key Lab of Submarine Geosciences and Prospecting Techniques, College of Marine Geosciences, Ocean University of China, Qingdao, China*
[2]*Laboratory for Marine Mineral Resources, Qingdao National Laboratory for Marine Science and Technology, Qingdao, China*

Correspondence should be addressed to Huaishan Liu; lhs@ouc.edu.cn

Received 18 March 2022; Accepted 30 August 2022; Published 25 September 2022

Academic Editor: Jin Qian

Marine vertical cable seismic (VCS) collects seismic waves by hydrophone array vertically suspended in seawater to prospect the offshore geological structure and monitor the reservoir. Due to its irregular source-receiver geometry, the primary imaging has narrow illustration coverage. Here, we proposed a cross-correlation transformation based on ghost wave interferometry. This method can transform the ghost reflections from the vertical cable seismic profile into the virtual surface seismic primaries just like those excited by the source and recorded by marine seismic towed-streamer below sea surface. After processing these virtual primaries with conventional method, we can obtain the ghost reflection imaging section with high resolution which effectively extend the illustration footprints in the subsurface. By application of this transform, virtual primaries are generated from the first-order ghost reflections of the actual VCS data. Then, migration of these virtual primaries provides a high-resolution image of hydrate-bearing sediments.

1. Introduction

Vertical cable seismic (VCS) exploration method makes use of vertical hydrophone arrays (VHA) to image subsurface target in geologically complex area [1–3]. Generally, several hydrophones are assigned on the seismic cable with equal interval, and this cable was vertically suspended in seawater under the joint action of buoys and anchor [4]. Actually, vertical cable is moored on the seafloor so that it can avoid some common marine noise such as swell in deep seawater. Consequently, VCS can provide high-quality seismic images beneath the seabed [4]. As vertical cable is deployed on the seabed, various marine sources can be used to shoot along seismic surveying line with any azimuth [5]. Compared with conventional marine seismic exploration, a truly 3D seismic data can be acquired by VCS with less cost [6].

Derived from defence research, the VCS method was successfully applied to conduct offshore seismic survey, for high-quality subsalt imaging [3, 7], for low-angle fault scarp imaging and assessment of remaining exploration potential [8], for hydrothermal deposit exploration [5], for seafloor massive sulphide survey [9–12], and for natural gas hydrate exploration [4, 13–15]. All these applications reveal that the VCS technique is an effective approach to exploiting and developing the complex offshore oil and gas fields, which can provide superior seismic image compared with conventional marine seismic method.

However, it is still open to debate about processing method for VCS dataset due to the irregular geometry in yield acquisition. The source and the hydrophones are at significantly different depths so it is invalid to process the original VCS dataset by conventional seismic data process methods. In view of this common issue, the Kirchhoff prestack migration can be used for the VCS imaging by the equivalent offset method (EOM) [16]. Accurate velocity fields can be estimated by performing velocity analyzing on common scatter point (CSP) gathers. In order to overcome the drawback of the irregular field geometry for VCS, the accurate velocity model can

be directly applied to image marine hydrate-bearing sediments by reverse time migration [4]. Besides, VSP processing method can be used for VCS data processing [17] because of its geometry similar to the VSP. However, it is necessary to provide an initial water velocity model for this method. The previous methods mainly make use of the primary reflections for the VCS imaging. Owing to the limited subsurface coverage, depth imaging by the primaries from VCS is unreliable. Alternatively, depth imaging with receiver-side ghost reflection can be implemented by mirror reverse time migration algorithm [18]. The key issue of this method is to obtain a reliable velocity field from the virtual surface seismic traces, which can be produced by implementing seismic interferometry on the VCS data.

In this paper, we present a new transform based on seismic interferometry by cross-correlation which converts VCS profile (VCSP) into virtual surface seismic profile (SSP). After processing actual VCS receiver gathers, we obtain a virtual SSP shot gathers by this transformation. Based on the conventional Kirchhoff time migration algorithm, we further obtain a high-quality seismic image from the virtual shot gathers. Although their amplitudes and phases are different from the conventional marine seismic dataset, this high-resolution imaging result still indicate the presence of gas hydrate with the distinct bottom simulating reflector (BSR).

2. Methodology

2.1. Seismic Interferometry by Cross-Correlation. The seismic interferometry originates from *acoustic daylight imaging*, whose main goal is to reconstruct a Green's function from the diffuse wavefield recorded at different receiver positions by cross-correlation [19–22]. For the exploration geophysicist, Green's function is called as the reflection response. Consequently, cross-correlation of records by two different receivers in an acoustic diffuse field produces a new reflection response [23]. It can be regarded as the reflection recorded by one of the receivers as if there were an impulsive source at the other receiver position. So far, seismic interferometry includes three algorithms, based on the cross-correlation [19, 24–26], the deconvolution [27–32], and the cross-coherence [33], respectively. Among them, cross-correlation is in widespread use as the earliest algorithm in the seismic interferometry.

Let us first review the cross-correlation algorithm used in seismic interferometry. Assume the source wavelet $W(s)$ is excited at s and the wavefield $u(r,s)$ is recorded at r by the receiver. Green's function from this wavefield is $G(r,s)$. Removing the additive noise [33], the wavefield $u(r,s)$ in the frequency domain can be given as

$$u(r,s) = W(s)G(r,s). \tag{1}$$

Consider $u(r_A,s)$ and $u(r_B,s)$ are the wavefields recorded at receiver position r_A and r_B, respectively. The cross-correlation of the two wavefields gives

$$C_{AB} = u(r_A,s)u(r_B,s) = |W(s)|^2 G(r_A,s)G^*(r_B,s), \tag{2}$$

where * denotes a complex conjugate. The above equation illustrates that the value of C_{AB} is dependent on the power spectrum of the source wavelet. According to the principle of seismic interferometry, we integrate the cross-correlation C_{AB} over a closed surface ∂V that includes all sources [33], giving

$$\oint_{\partial V} C_{AB}ds = \left\langle |W(s)|^2 \right\rangle \oint_{\partial V} G(r_A,s)G^*(r_B,s)ds, \tag{3}$$

where $\langle |W(s)|^2 \rangle$ is the average of the power spectral for the source wavelet. This equation provides Green's function between the two receivers with a multiplicative constant, approximately.

2.2. VCSP-to-SSP Transformation. New seismic events can be generated by cross-correlation of different seismic traces, whose ray paths and traveltimes are shorter than that in the raw traces [34]. In order to derive VCSP-to-SSP transform from the above issue, consider the example shown in Figure 1. Let $G(r_A,s) = e^{i\omega\tau_{SRGH}}$ represent the receiver-ghost wave with traveltime τ_{SRGH} in the left panel and let $G(r_B,s) = e^{i\omega\tau_{GH}}$ represent the direct wave with traveltime τ_{GH} in the middle panel. Here, we assume that the reflection coefficient is 1.0 and the above-mentioned Green's functions are all normalized by the spherical spreading factor [34]. Substituting these Green's function into equation (2) gives

$$\begin{aligned} C_{AB} &= |W(s)|^2 \left(e^{i\omega\tau_{SRGH}} \cdot e^{-i\omega\tau_{GH}}\right) = |W(s)|^2 \left[e^{i\omega(\tau_{SRGH}-\tau_{GH})}\right] \\ &= |W(s)|^2 \cdot e^{i\omega\tau_{SRG}}, \end{aligned} \tag{4}$$

where $e^{i\omega\tau_{SRG}}$ represent the normalized Green's function of an SSP primary with two-way traveltime τ_{SRG}. This equation reveals that the correlation of a pair of traces creates a new trace with shorter ray paths and traveltimes. As shown in Figure 1, the correlation of a ghost reflection along the ray path SRGH with a direct arrival along the ray path GH removes the common traveltime of the receiver-ghost wave along the ray path GH and redatums the hydrophone to be on the sea surface. Consequently, it produces a *virtual* surface seismic primary reflection in surface seismic surveying. In this case, the vertical cable seismic data have been transformed into the surface seismic data. This *virtual* surface seismic data is equivalent to the conventional seismic traces recorded by a configuration of receivers and sources near the sea surface [34], such as conventional marine towed-streamer seismic surveying. In a word, VCS ghost reflections can be kinematically transformed into SSP primaries, using seismic interferometry by cross-correlation.

3. Results and Discussion

3.1. Data Processing. In 2017, we obtained a 3D VCS dataset natural gas hydrate exploration in Shenhu area, South China Sea, using the distributed vertical cable seismic (DVCS) acquisition system [4], conducted by the Guangzhou Marine Geological Survey Bureau [15]. This dataset consists of 12

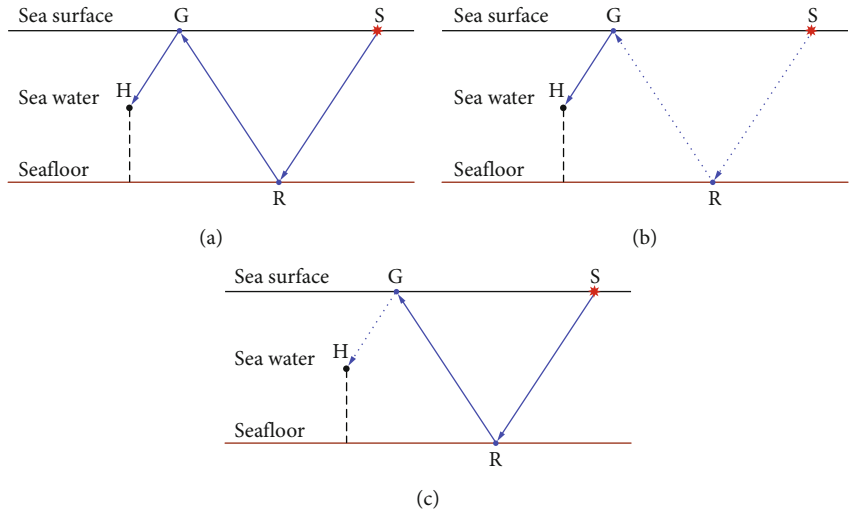

Figure 1: Cross-correlation of (a) a VCSP ghost wave with (b) a VCSP direct wave yields the SSP primary (c).

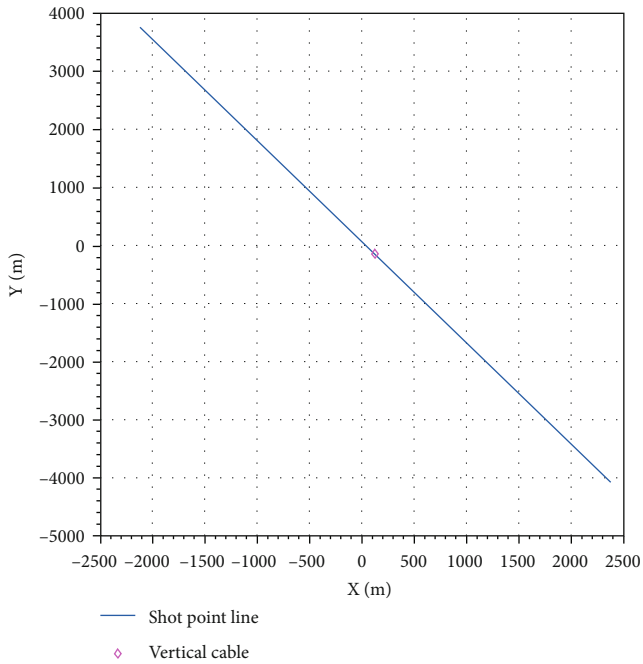

Figure 2: Location of line 39 and vertical cable.

common receiver gathers with shots distributed every 25 m from 60 different shot lines whose space is 100 m. The depth range of receivers is from 765 m to 1040 m below sea surface with interval 25 m. And the sample interval of the VCS dataset is 0.25 ms.

Here, we mainly use receiver ghost reflection from the shallowest hydrophone to image hydrate-bearing sediments across the line 39 (Figure 2), which is the closest line to the VC. The length of this line is 20 km approximately, with 801 shots in total. In this paper, we used 360 shot gathers to image subsurface structure, whose shot point number is from 1261 to 1621. And the VC is located at seafloor below the middle between shot 1440 and shot 1441. After band-pass filtered [4], this common receiver gather from the shallowest hydrophone is shown in Figure 3, whose dominant frequency varies from 10 Hz to 300 Hz approximately. It is of high resolution and signal-to-noise ratio, clearly showing the direct wave, seafloor reflection, and receiver ghost reflection (more generally, the free-surface multiple). Additionally, enhanced reflections (ERs) arrive later than the seafloor reflection. They are of adequate energy so that it is comparable to the energy of the seafloor reflection. Similarly, another one arrives later than the receiver ghost reflection which we will transform into a virtual SSP primary using seismic interferometry by cross-correlation.

In order to form an interferogram with high quality, some preprocessing steps are performed on the common receiver gather in VCS data, such as band-pass filter and wavefield separation. After that, the first-order receiver ghost reflections are correlated with the direct waves and produce the virtual surface seismic shot gathers shown in Figure 4. If we do not perform the wavefield separation of the VCS data, all the seismic waves should be correlated with the direct waves. Consequently, it will bring about cross terms such as cross-correlation of the primaries of real VCS data with the direct waves. Figure 5(b) shows the effect of the so-called cross terms. Mass of events appears between the two green dashed lines and seems to be reflections from different layers. In fact, the reflections related to stratum will not appear on the top of the virtual seafloor reflections. What is worse, it will make velocity analysis of virtual seafloor reflections unreliable and degrade the quality of seismic imaging. Figure 5(a) shows a part of the seismic interferogram after wavefield separation. Virtual seafloor reflection and enhanced reflections appear in the new shot gathers with high signal-to-noise ratio.

3.2. Interferometric Imaging Result. Figure 4 shows the virtual SSP produced by the receiver gather from the top hydrophone deployed in the vertical cable. Similar to the conventional marine towed-streamer seismic profile, the events of direct wave and seafloor reflection are prone to distinguish from other events on this seismic section. In addition, virtual enhanced reflections (ERs) arrived later than

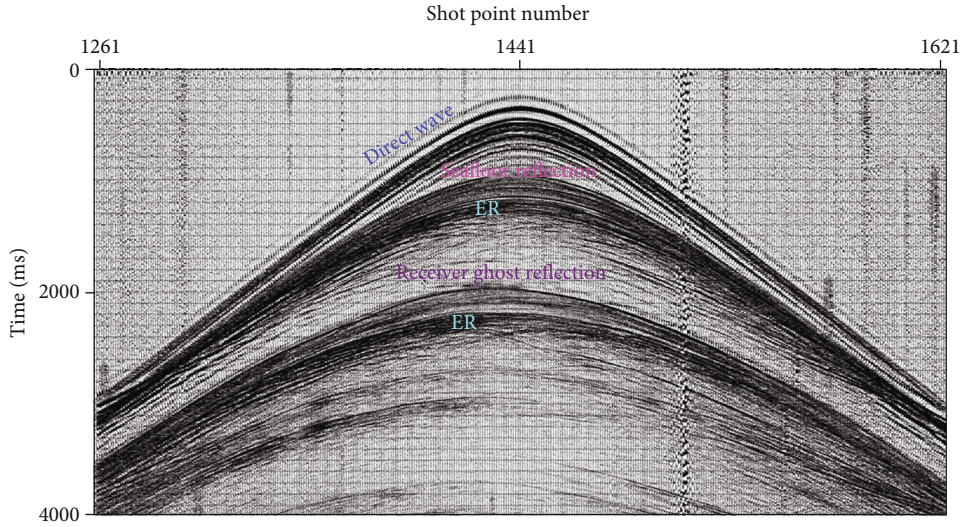

Figure 3: The filtered receiver gathers from the shallowest hydrophone.

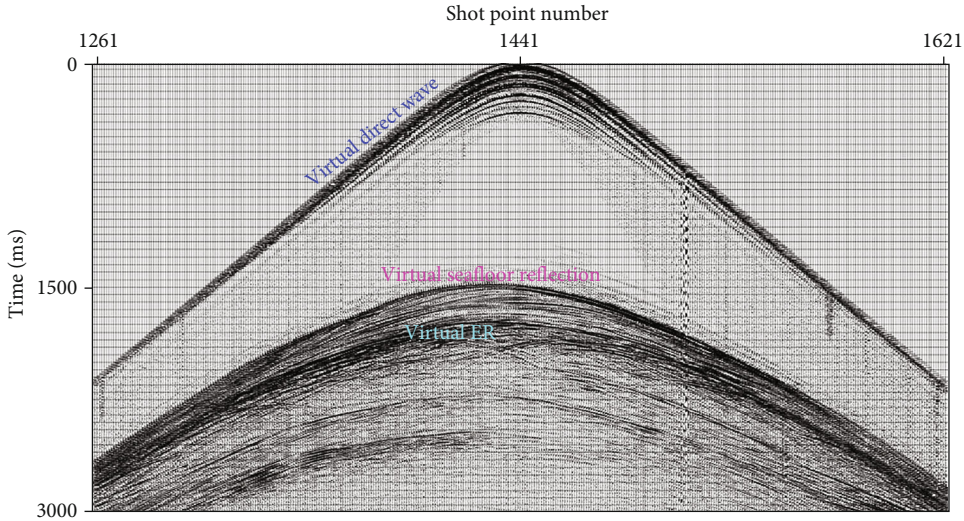

Figure 4: Virtual shot gathers obtained by correlating receiver ghost reflection with the direct wave.

the seafloor with larger amplitudes. What is more, the seismic resolution and signal-to-noise ratio is preserved well. However, the amplitudes of all these events on this seismic section are different from the conventional seismic profile, and they are only the cross-correlation values which indicate the variation of amplitude energy.

After transforming VCSP ghost reflections into virtual SSP, we can perform the conventional seismic processing method on this SSP gathers, such as velocity analysis, NMO correction, and migration. Finally, the SSP gathers is migrated by the Kirchhoff diffraction-stack algorithm, and we obtain the imaging section as shown in Figure 6. Similar to the migration image of surface seismic traces, it clearly shows seafloor reflection, sediment waves, and bottom simulating reflector which are parallel to the seafloor. In addition, the seismic resolution is preserved as well.

3.3. Discussion. The VCSP-to-SSP transform creates a set of the virtual SSP data using cross-correlation of ghost reflections and the direct waves in VCS dataset. Here, this transform is used to convert the first-order ghost reflections into the SSP primaries for the purpose of hydrate-bearing sediment imaging from VCS dataset.

The chief benefit of this VCSP-to-SSP transform is the superillustration of the subsurface. In theory, seismic imaging with multiples can extend the subsurface coverage which is wider than that of seismic imaging with primaries. In this paper, we mainly use the first-order ghost reflections to extend the illustration footprint for VCSP imaging. As shown in Figure 6, the coverage area of the VCSP multiple imaging result with the first-order ghost waves is over a 5625 m region, which is approximately 5 times than that of the VCS primary imaging result in [4]. Another benefit is that the vertical hydrophone

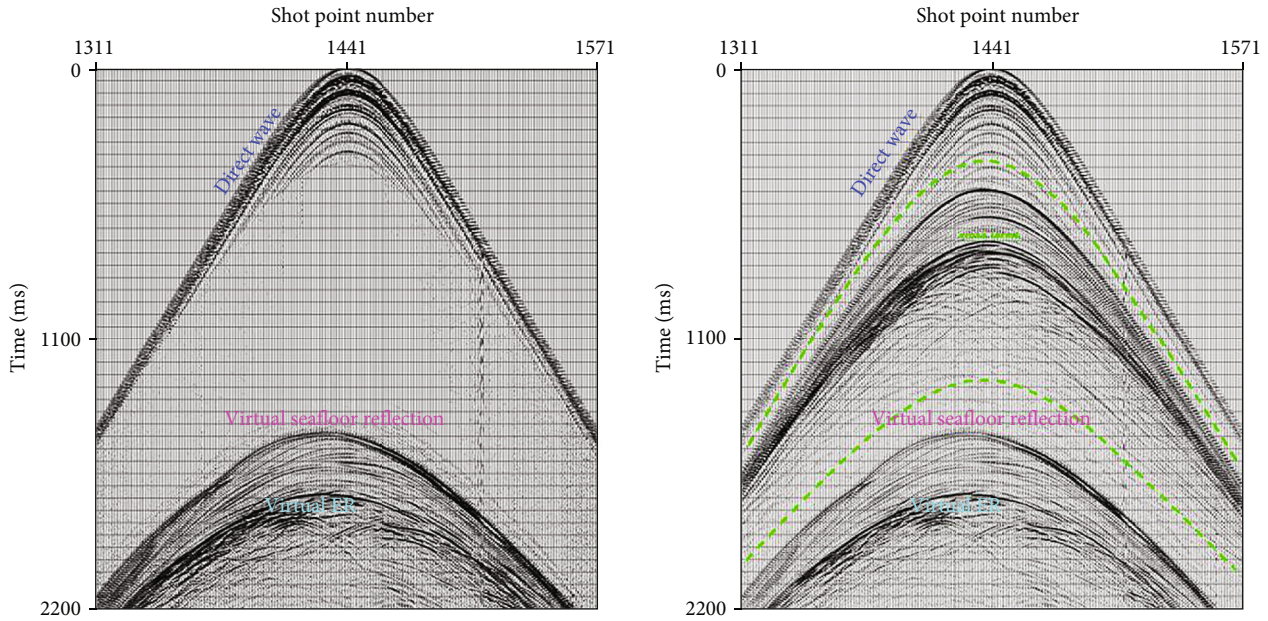

Figure 5: Interferogram ((a) cross-correlation of the direct wave with ghost waves and (b) cross-correlation of the direct wave with all waves).

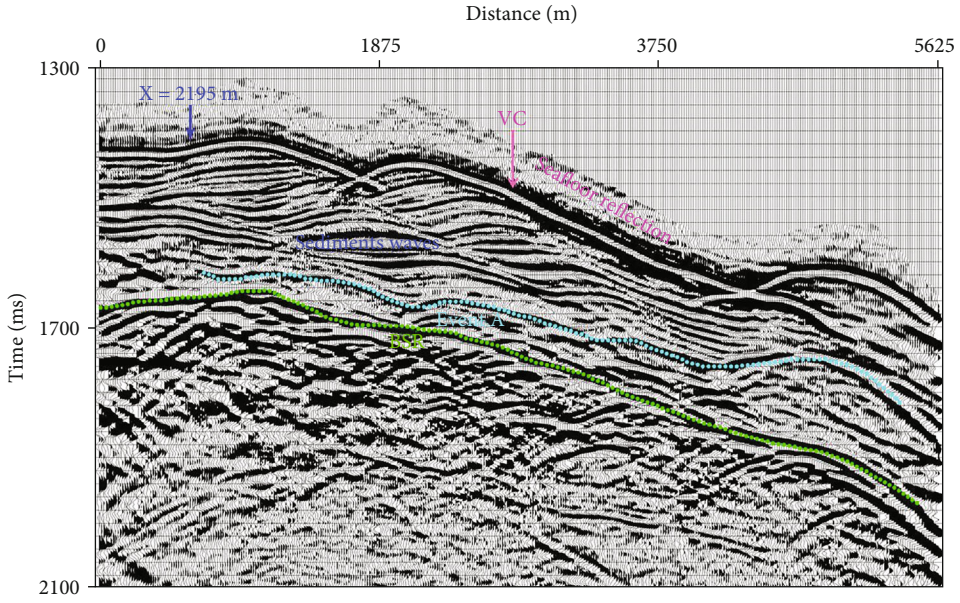

Figure 6: Ghost reflection imaging result with the above-mentioned virtual SSP gathers.

array suspended in the seawater, after VCSP-to-SSP cross-correlation transform, is redatumed upward to the sea surface. This means that the redatumed traces can be effectively imaged with higher resolution. Finally, no velocity model is needed for this transform. The VCSP ghost reflections can be directly transformed into the virtual SSP traces by the cross-correlation transformation, without known source excitation times and hydrophone locations. It provides a significant improvement in VCS data processing for its irregular yield geometry. Because it is extremely difficult to accurately position the hydrophones in the seawater.

However, there are still several problems for the VCSP-to-SSP transform. A key problem is the truncation artifacts in the virtual SSP data generated from the VCSP by seismic interferometry. It is caused by the limited source and receiver arrays of the actual VCS data. Consequently, only some of the events in the virtual SSP represent the specular reflections accurately. Another problem with this VCSP-to-SSP transform is that

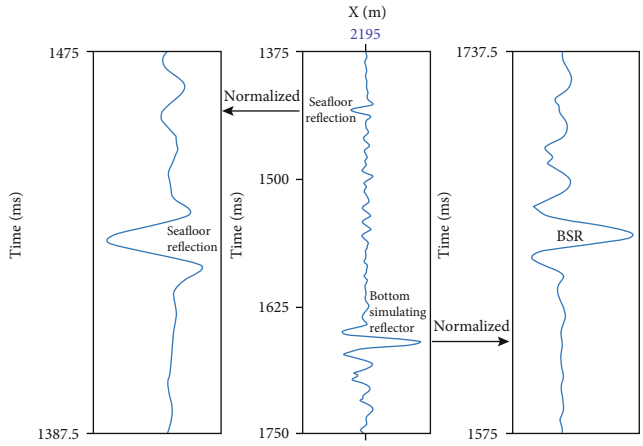

Figure 7: Seismic trace at $X = 2195$ m on the first-order ghost imaging section in Figure 6.

seismic interferometry by cross-correlation does not account for the rock attenuation. But the seismic waves suffer from energy attenuation while propagating in the Earth which is anelastic in reality. This means that the virtual SSP obtained by the VCSP-to-SSP transform will not have the correct amplitudes. Therefore, it seriously lowers the signal-to-noise ratio of the virtual surface seismic primaries.

Although the retrieved amplitudes in the virtual SSP are not exactly predicted by the above transformation, the phases of these amplitudes are still correct according to the equation (4). This is because the reflections which are in phase can bring about constructive interference and the reflections with out of phase result in destructive interference. As shown in Figure 6, an event parallel to the seafloor can be recognized by the reversed phase with respect to the seafloor reflection. It is similar to the bottom simulation reflector (BSR) presented in the conventional surface seismic profile. Consequently, this event can also be regarded as the BSR in a way. Figure 7 shows the seismic trace located at $X = 2195$ m in the first-order ghost imaging section. It is observed that the so-called BSR has greater amplitude than that of the seafloor reflection. Moreover, the phases of these two reflections are reversed polarity.

4. Conclusions

The VCS survey is a promising technique to hunt for natural gas hydrates in deep water. Owing to its unique geometry, the primary reflection imaging provides narrow illustration of the subsurface. Alternatively, receiver ghost reflections can be used to image the geological structures beneath the sea bottom in order to extend the illustration coverage of the subsurface reflectivity. In this paper, we implement the seismic interferometry by cross-correlation to the VCSP shot gathers and transforms the first-order ghost reflections into virtual SSP primaries kinematically. Performing the conventional migration algorithm on these virtual primaries produces the high-quality imaging section with respect to the submarine reflectivity. This imaging result clearly shows reflection events of hydrate-bearing sediments with high resolution in spite of the inaccurate amplitudes. Therefore, we believe that seismic interferometry by cross-correlation is an effective way to process the VCS data.

Data Availability

The raw data used to support the conclusions of this study are available from the corresponding author upon request.

Conflicts of Interest

The authors declare that they have no conflicts of interest.

Acknowledgments

The authors would like to thank the Guangzhou Marine Geological Survey Bureau of Chinese Geological Survey Bureau for conducting the vertical cable seismic acquisition experiment in Shenhu area, South China Sea. This work was financially supported by the National Natural Science Foundation of China (Grant Nos. 91958206 and 41204087), the National High-Tech Research and Development Program (Grant No. 2013AA092501), and the China Scholarship Council.

References

[1] P. M. Krail, "Case history vertical cable 3D acquisition," in *53rd EAGE Conference and Exhibition*, Liverpool, UK, 1991.

[2] P. M. Krail, "Sub-salt acquisition with vertical cable," in *63rd EAGE Conference and Exhibition*, Amsterdam, Holland, 1993.

[3] P. M. Krail, "Vertical cable as a subsalt imaging tool," *The Leading Edge*, vol. 13, no. 8, pp. 885–887, 1994.

[4] L. Wang, H. Liu, Z. Wang, J. Zhang, L. Xing, and Y. Yin, "Reverse time migration of vertical cable seismic data to image hydrate-bearing sediments with high resolution," *Frontiers in Earth Science*, vol. 9, article 751202, 2021.

[5] E. Asakawa, F. Murakami, and Y. Sekino, "Development of vertical cable seismic system," in *74th EAGE Conference and Exhibition*, Copenhagen, Denmark, 2012.

[6] H. J. Wang, *Seismic Imaging and Anisotropic Inversion Using Vertical Cable Data*, doctor's thesis, University of Edinburgh, Edinburgh, 2003.

[7] P. M. Krail, "Vertical cable marine seismic acquisition," in *Offshore Technology Conference*, Houston, USA, 1997OTC-8315-MS.

[8] P. E. Leach, "Strathspey vertical-cable seismic survey: a North Sea first," in *Offshore Europe Conference*, pp. 333–347, Aberdeen, UK, 1997.

[9] E. Asakawa, F. Murakami, H. Tsukahara, and S. Mizohata, "Vertical cable seismic (VCS) survey for seafloor massive sulphide (SMS) exploration," in *76th EAGE Conference and Exhibition*, Amsterdam, Holland, 2014.

[10] E. Asakawa, F. Murakami, H. Tsukahara, and S. Mizohata, "Development of vertical cable seismic (VCS) system for seafloor massive sulfide (SMS)," in *2014 Oceans-St. John's*, pp. 1–7, St. John's, NL, Canada, 2014.

[11] E. Asakawa, F. Murakami, H. Tsukahara, S. Mizohata, and K. Tara, "Vertical cable seismic surveys for SMS exploration in Izena Cauldron, Okinawa-Trough," in *Oceans 2015*, pp. 1–5, Genova, Italy, 2015.

[12] E. Asakawa, K. Tara, F. Murakami, H. Tsukaraha, and S. Mizohata, "Vertical cable seismic (VCS) survey for buried hydrothermal sulfide deposit," in *Offshore Technology Conference*, Houston, USA, 2016.

[13] X. Wang, L. Liang, and Z. Wu, "Research on seismic wave attenuation in gas hydrates layer using vertical cable seismic data," *Pure and Applied Geophysics*, vol. 175, no. 10, pp. 3451–3462, 2018.

[14] L. Xing, H. S. Liu, X. L. Zheng et al., "Phase characteristic analysis of continuous depth air-gun source wavelet," *Journal of Ocean University of China*, vol. 15, no. 5, pp. 815–824, 2016.

[15] X. Wang, Q. Zhao, Z. Wu, B. Liu, and T. Huang, "Research on vertical cable seismic multiples imaging processing," *Arabian Journal of Geosciences*, vol. 12, no. 4, pp. 1–5, 2019.

[16] J. C. Bancroft and Y. Xu, "Equivalent offset migration for vertical receiver arrays," *CREWES Research Report*, vol. 10, no. 11, pp. 1–6, 1998.

[17] J. Bailey, E. Asakawa, M. Humphries, and K. Tara, "Vertical cable seismic (VCS) processed using VSP methods," *4th EAGE Workshop on Borehole Geophysics*, 2017, pp. 1–5, Abu Dhabi, United Arab Emirates, 2017.

[18] E. Jamali, M. Katou, K. Tara, E. Asakawa, and H. Mikada, "Mirror reverse time migration using vertical cable seismic data for methane hydrate exploration," *Geophysics*, vol. 84, no. 6, pp. B447–B460, 2019.

[19] J. F. Claerbout, "Synthesis of a layered medium from its acoustic transmission response," *Geophysics*, vol. 33, no. 2, pp. 264–269, 1968.

[20] S. Cole, *Passive Seismic and Drill-Bit Experiments Using 2-D Arrays*, Ph.D. thesis, Stanford University, 1995.

[21] J. E. Rickett and J. F. Claerbout, "Acoustic daylight imaging via spectral factorization: helioseismology and reservoir monitoring," *The Leading Edge*, vol. 18, no. 8, pp. 957–960, 1999.

[22] G. T. Schuster, J. Yu, J. Sheng, and J. Rickett, "Interferometric/daylight seismic imaging," *Geophysical Journal International*, vol. 157, no. 2, pp. 838–852, 2004.

[23] K. Wapenaar, D. Draganov, and J. Robertsson, "Introduction to the supplement on seismic interferometry," *Geophysics*, vol. 71, no. 4, p. SI1, 2006.

[24] K. Wapenaar, "Synthesis of an inhomogeneous medium from its acoustic transmission response," *Geophysics*, vol. 68, no. 5, pp. 1756–1759, 2003.

[25] A. Bakulin and R. Calvert, "Virtual source: new method for imaging and 4D below complex overburden," *74th Annual International Meeting*, vol. 23, pp. 112–115, 2004.

[26] P. Roux, K. G. Sabra, P. Gerstoft, W. A. Kuperman, and M. C. Fehler, "P-waves from cross-correlation of seismic noise," *Geophysical Research Letters*, vol. 32, no. 19, 2005.

[27] R. Snieder and E. S. Afak, "Extracting the building response using seismic interferometry: theory and application to the Millikan library in Pasadena, California," *Bulletin of the Seismological Society of America*, vol. 96, no. 2, pp. 586–598, 2006.

[28] I. Vasconcelos and R. Snieder, "Interferometry by deconvolution: part 1 — theory for acoustic waves and numerical examples," *Geophysics*, vol. 73, no. 3, pp. S115–S128, 2008.

[29] I. Vasconcelos and R. Snieder, "Interferometry by deconvolution: part 2 — theory for elastic waves and application to drill-bit seismic imaging," *Geophysics*, vol. 73, no. 3, pp. S129–S141, 2008.

[30] I. Vasconcelos, R. Snieder, and B. Hornby, "Imaging internal multiples from subsalt VSP data — examples of target-oriented interferometry," *Geophysics*, vol. 73, no. 4, pp. S157–S168, 2008.

[31] K. Wapenaar, E. Slob, and R. Snieder, "Seismic and electromagnetic controlled-source interferometry in dissipative media," *Geophysical Prospecting*, vol. 56, no. 3, pp. 419–434, 2008.

[32] K. Wapenaar, J. van der Neut, and E. Ruigrok, "Passive seismic interferometry by multidimensional deconvolution," *Geophysics*, vol. 73, no. 6, pp. A51–A56, 2008.

[33] N. Nakata, R. Snieder, T. Tsuji, K. Larner, and T. Matsuoka, "Shear wave imaging from traffic noise using seismic interferometry by cross-coherence," *Geophysics*, vol. 76, no. 6, pp. -SA97–S106, 2011.

[34] G. T. Schuster, *Seismic interferometry*, Cambridge University Press, New York, 2009.